Meas. Sci. Technol. **11** (2000) 568–575. Printed in the UK PII: S0957-0233(00)09741-1

Particle positioning from CCD images: experiments and comparison with the generalized Lorenz–Mie theory

J A Guerrero†, F Mendoza Santoyo†, D Moreno†, M Funes-Gallanzi‡ and S Fernandez-Orozco§

† Centro de Investigaciones en Optica AC, Loma del Bosque 115, Colonia Lomas del Campestre, León, Guanjuato 37150, Mexico
‡ Instituto Nacional de Astrofísica Óptica y Electrónica (INAOE), Tonantzintla, Puebla, Mexico
§ Arquitectura en Sistemas Computacionales Integrales, SA de CV, Guadalajara, Jalisco, Mexico

E-mail: chon@foton.cio.mx (J A Guerrero), fmendoza@foton.cio.mx and gallanzi@inaoep.mx

Received 19 November 1999, in final form 4 February 2000, accepted for publication 14 March 2000

Abstract. This paper describes the experimental imaging of a spherical particle diffraction pattern obtained in back, forward and side scattering configurations, using illumination from three different beam shapes. The experimental problems encountered for each of the viewing configurations and the theoretical analysis of the diffraction pattern of the particle on its image plane using the generalized Lorenz–Mie theory are discussed. The images obtained are quantitatively compared with calculated results and implications for particle position estimation are discussed.

Keywords: diffraction pattern, back, forward and side scattering, particle position estimation, particle image velocimetry, velocimetry

1. Introduction

Conventional velocimetry has an intrinsic limitation because it yields two-dimensional data, neglecting the third velocity component. For this reason, three-dimensional particle image velocimetry (PIV) has recently evolved as an area of research [1–16], with success at the cost of increasing complexity in its methodology. The increasing complexity and the limited optical access found in most industrial applications mean that many of the three-dimensional PIV techniques, although they are of academic interest, cannot be used in practical industrial applications. Some of the techniques used involve scanning light sheets, stereoscopic views, holographic recording, parallel light sheets, graded intensity light-sheets, or combinations thereof.

For practical applications restricted viewing eliminates stereoscopic approaches. Lack of robustness and the difficulty of performing an experiment make conventional holography an unattractive option due to the fact that it involves a wet developing process and hence is very slow to yield results. However, its large depth of field and storing capacity make it a technique that should, given the correct environment, be used. When holography is used the hologram is interrogated with the aid of cameras mounted on a high-precision three-dimensional positioning system, to resolve position on the basis of particle image information. Scanning light sheets are difficult to obtain for restricted optical access and high speeds, so they have not been tried under industrial conditions.

CCD cameras are nowadays being used as image recording media. Restricted optical access to flows of interest, such as those found in turbomachinery, means that often only one camera can be accommodated. An extension to the high-accuracy techniques for three-dimensions, exploiting the digital representation of particle images in intensity as well as spatially, is described in previous work [17]. The analysis of digital PIV data typically involves two quantization steps, namely spatial and intensity quantization. It is of crucial importance to have reliable error bounds and a sufficiently accurate estimate of the particle position, taking into consideration both types of quantization. The approach of using the Gaussian profile of the particle images to yield position estimates of sub-pixel accuracy has resulted in robust measurements being taken to an accuracy of a tenth of a pixel and 1% in velocity for the in-plane velocity, even in hostile industrial environments. The out-of-plane velocity estimate can be derived from

0957-0233/00/050568+08$30.00

the change in the ratio of amplitude to variance (known as the depth factor) of the Gaussian form, as a particle traverses the beam profile. However, such measurements are crucially dependent not only on an accurate position estimate but also on an equally accurate estimate of the amplitude and variance. Gaussian profile fitting using a Nelder–Meade optimization method was not capable of providing the required accuracies. Therefore, a development of the 'locales' approach to position estimation was presented in order to achieve the desired objective of high accuracy PIV measurements. This approach makes use of the fact that, by considering the possible digital representations of the Gaussian particle profile, regions of indistinguishable position can be derived. These positions are referred to as 'locales'. By considering the density, distribution and shape of these locales, the available precision can be estimated and a high accuracy for the in-plane velocity can be obtained; while at the same time providing high-accuracy estimates of the depth factor. This work describes the implementation of an efficient algorithm to provide velocity estimates, together with a discussion of the required constraints imposed on the imaging. The algorithm was used to map an experimental transonic flow field of the stator trailing edge region of a full-size annular cascade with an estimated error of 0.5%. The experimental results were found to be in good agreement with a previously reported steady state viscous calculation and PIV mapping. This work has been extended to a model, using simplified Fraunhofer particle diffraction, for pattern-matching low-magnification three-dimensional particle positioning, whereby particles are illuminated by monochromatic light which is to appear elsewhere [18]. Detailed theoretical models will then be useful for examining the effect of changing the aperture size on the observed particle images, the nature of the variation of the image quality with the degree of particle defocus, etc. The most advanced such model is that based on generalized Lorenz–Mie theory (GLMT) which takes into account typical wavefronts occurring in velocimetry applications, such as that of a light sheet which is elliptical, rather than the simple plane wavefront assumption of classical Lorenz–Mie theory (LMT). These models need to be validated against experimental data, so that they may be used to find out which parameters are more important and therefore require further modelling, in order to achieve a quantitatively accurate representation of diffraction for a given position and given particle characteristics. This is the overall subject of this paper.

The case of a spherical absorbing particle illuminated with monochromatic coherent light is considered. Three different illumination wavefront shapes and three viewing positions are used and their relative merits are studied. The data obtained have been used to validate a model of particle scattering. An experimental 18 μm glass sample image is quantitatively compared with the calculated image for a Gaussian wavefront in forward scattering. This sample image in this viewing configuration has been chosen and described by a number of other authors [19–23] and therefore was chosen as the sample case for the present work.

2. The formulation of the problem

Adrian and Yao [24] first proposed using a quadrature to derive a nominal particle image diameter d_e according to

$$d_e = (M^2 d_p^2 + d_s^2)^{1/2} \tag{1}$$

where M is the lateral magnification of a lens and d_p is the particle diameter. In this equation

$$d_s = 2.44(M + 1)\lambda f/D \tag{2}$$

is the diameter of the point response function of a diffraction-limited lens measured at the first dark ring of the intensity distribution of the Airy disc, λ is the wavelength of the laser light used and the focal length of the lens divided by the aperture diameter is f/D. As defined here, d_s may also be regarded as equal to twice the mean diameter of a speckle. Equation (1) shows the combined effects of magnification and image blurring and is an approximate quadrature determining the final diameter of the image. If the point response function and the geometrical image were both Gaussian, equation (1) would be exact. In fact a Gaussian intensity distribution has been used widely as an adequate approximation to the Airy intensity distribution for velocimetry applications. Hence, equation (1) was used as an approximation, assuming that the geometrical image distribution is not too different from a Gaussian distribution function.

This approach represents a compromise between geometrical optics and a simplified approximation to LMT. However, the former is valid only when the wavelength λ is much smaller than a length given by the standard deviation of the surface roughness (scattering size), i.e. for optically smooth surfaces, and the latter is valid only when the particle is illuminated by a plane wave. The plane wave assumption holds when the scattering size of the particle is small compared with the characteristic dimensions of the incident beam; however, under many cases this condition is not satisfied. Even if the plane wave assumption holds in a velocimetry set-up, the orientation of this wavefront relative to the viewing camera generally changes across the field of view in such a way that major corrections are required for each particle's scattered image because particles are far away from the optical axis and intensity distributions are not uniform over the whole image. This effect need not be readily apparent in applications involving thin light sheets and small particles viewed by imaging lenses focused on said light sheet, where the particle image approximates a Gaussian function and is only a few pixels in diameter. However, when larger illumination depths are used the particle image diameter quickly extends substantially. Even for thin light sheets, for which the CCD camera is adjusted so that it saturates at the higher light intensities, diffraction rings become visible and these vary substantially with the particle position within the light sheet down to a movement of as little as 20 μm.

An accurate analysis of the resulting diffraction field relies, for any position in the illuminated field, on the GLMT. The GLMT deals with arbitrarily shaped incident beams [25, 26]. It is thoroughly covered in a complementary paper applied to velocimetry [27], in which the full mathematical approach is described.

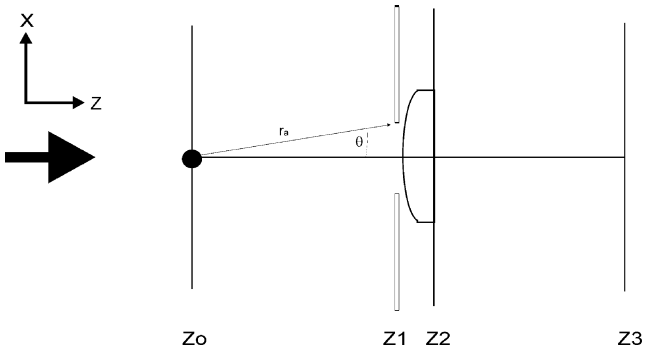

Figure 1. The simplified imaging layout.

Simplifications in formulating the physical problem to be solved were considered, e.g. assuming a particle to be a point function. However, such a treatment does not consider the complex refractive index of a particle and considers neither the incident laser power nor the various intensity distributions exhibited by particles that are an equal distance away from focus on opposite sides of the focal plane. The latter aspect is of crucial importance in making such an approach worthwhile, since, if the position of particles behind and in front of the focal plane cannot be distinguished, the approach would be meaningless.

Initially, we devised a theoretical model which allows calculation of the image produced by a spherical absorbing particle illuminated with monochromatic light, including the amount of light energy falling onto a CCD sensor.

The imaging system under consideration has been described in detail in previous work by other authors [19, 20] and is summarized in figure 1. This system was used as a starting point to validate the theoretical model and experimental results†. An object located on the plane z_0 is illuminated with a He–Ne laser. The object image is formed by letting the scattered light go through a plano-convex lens ($f = 90$ mm, $D = 32$ mm) onto a sensor (in the plane z_3). The image captured is then sent to a frame grabber.

Assuming that the laser–droplet interaction can be modelled as a linearly polarized plane wave incident on a spherical absorbing particle, the electromagnetic field distribution at any point can be obtained using the classical LMT [28, 29]. These equations give the correct solution for the electromagnetic field at every point within the aperture located at z_1. The scalar diffraction theory outlined by Goodman [30] assumes that the x-component of the electrical field will be the only significant electrical field component throughout the imaging system and makes use of the Fresnel approximation to propagate the field to the image plane.

The actual physical problem depicted in figure 1 can be further simplified on the basis of several experimental observations. Diffraction effects due to a given aperture size for the imaging system may be neglected and, if the aperture decreases, the effective lens diameter, f/D, is increased. As the aperture size becomes smaller, however, diffraction effects should be taken into account and the model needs to include the shape of the aperture.

† The software was kindly made available by Professor Alexander of the Center for Electro-Optics in the Mechanical Engineering Department at the University of Nebraska–Lincoln.

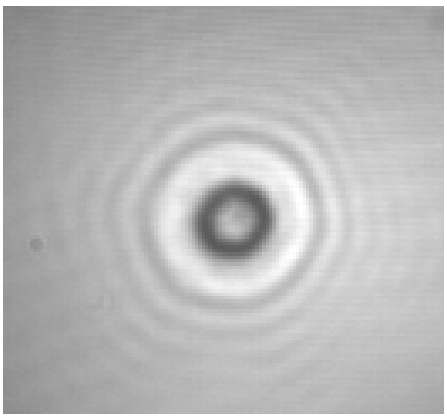

Figure 2. The aperture effect of the six-blade commercial lens on particle scattered images. The image was taken with a SIGMA 90 lens, $f = 8$, for a polystyrene particle diameter of 18 μm and $\lambda = 632.8$ nm. The slight asymmetry is due to camera misalignment.

3. The theoretical model

The theory for a plane wave scattered by a spherical, isotropic, homogeneous, non-magnetic particle can be found in the literature [28, 29]. More advanced theoretical and experimental techniques may be used, but these depend on the solution to the general problem in which the scattering centre is illuminated by a laser beam, leading to the so-called GLMT [25, 26]. The Gaussian beam case has been extensively investigated and applied in the analysis and improvement of practical devices such as phase Doppler systems. However, these techniques had not previously been applied to velocimetry. Velocimetry requires the application of GLMT techniques to the case of a beam with an elliptical cross-section, which is the case of laser sheets.

Beginning with the classical treatment, the geometry for a simplified model was used. The experimental results using the classical LMT treatment, however, proved insufficient to provide high accuracy three-dimensional particle positioning and therefore the algorithm was extended to use a GLMT treatment [31] for a plane wavefront, Gaussian beam and a light sheet.

Moreover, experiments indicated the need to consider third-order Seidel aberrations in a typical lens used for velocimetry, such as a 90 mm SIGMA Macro, in order to increase the accuracy of the model and thereby the accuracy of the particle positioning algorithm. The aberrations included in the model are sphericity and coma.

Currently, aperture shapes other than circular are being considered, for instance typical commercial lenses have six blades to form an aperture. It has been shown that, when the aperture size is reduced, the effect produced needs to be taken into consideration and at low apertures the particle image is degraded as shown in figure 2.

The GLMT code produced for this research work was verified in a number of different ways, namely the Legendre polynomials were derived and compared with established algorithms [33]; the numerical integration algorithm was a simple Gauss quadrature scheme, the Ricatti–Bessel coefficients were derived from the work in [33] for convenience, though faster more modern algorithms exist.

For the case of a plane wavefront, the calculations were compared with the experimental results and calculations of Schaub *et al* [20]. Gaussian wavefronts were also compared with experimental/computational results and found to be in good agreement. The GLMT algorithm itself was extensively compared with the results discussed by Gouesbet *et al* and found to coincide well, within computational limitations [25, 31, 34]. There are no experimental data for comparison of the diffraction image arising from elliptically shaped wavefronts. Therefore, the GLMT predictions could only be compared with the experimental images to be shown here.

To illustrate the differences among the three illumination schemes, figure 3 shows the intensity distribution as a function of the viewing angle for a particle of diameter 5 μm, using the GLMT. According to figure 3, at 0° (forward scattering) and 180° (back scattering) the distribution is symmetrical for a given ratio in three co-ordinates, so the calculation for the particle diffraction pattern is easier to perform than is that at 90° or 270° (side scattering), for which the distribution shape of the diffraction pattern is not symmetrical and the calculation needs to be performed for each point in the aperture and the radial symmetry simplification does not apply. Moreover, figure 3 shows the vast differences in intensity between viewing positions and illumination wavefronts. Therefore, it is advantageous to carry out bespoke tuning of the CCD camera, including switching to manual gain from automatic gain, to exploit to the full the dynamic range available from the CCD. Finally, predictions using GLMT confirmed the observation made by other authors [19–23] that particle images on either side of the focus plane are different.

4. The experimental arrangement

The experimental set-up devised allows recording of forward scattering, as in [20], with which the results were compared, backward scattering and the more conventional orthogonal viewing with a thin light sheet used in PIV. Figure 4 shows this experimental set-up for the three configurations. Figure 4(A) shows a view of the particle in the conventional PIV side-scattering mode. The slide was antireflection coated to optimize the signal-to-noise ratio (SNR). In order to view the same particle in back-scattering mode, a polarizing beam splitter was used in conjunction with a quarter-wave retarder plate like in figure 4(B). Figure 4(C) shows the typical forward-scattering configuration.

Three types of illumination were used, a plane wavefront as in classical LMT, a Gaussian wavefront such as those used in particle sizing and a light sheet as in PIV. The incident beam's power is taken into account by the model used. So, although a Nd:YAG laser is normally used, rather than a He–Ne laser (operating at 20 mW and $\lambda = 0.6328$ μm) as was employed for these tests, the difference only results in a change in the amount of energy delivered to the particle and a consequent change in the particle scattered field energy which is expressed in lux in the code, in order to allow simpler calibration of the CCD camera response. It is worth mentioning that the code developed does not make any simplifying assumptions based on size. Therefore, if the code could be validated for larger particles, it can also be applied to micrometre-sized particles, as are commonly employed in PIV. Larger particle sizes were chosen for convenience of handling only.

Various kinds of particles and sizes were investigated. These ranged from water droplets [35] and glass spheres to pollen. Actual particle sizes were verified by microscopic techniques. Available sizes ranged from 4 to 150 μm.

5. Results and discussion

The initial part of the research work reported here consisted of carrying out a first approximation simulating particles as pin holes and observing the variation of the diffraction pattern as defocus was applied. For these tests the arrangement used was for a forward scattering experiment as reported by other workers [19, 20]. The laser beam was collimated to a diameter of approximately 2 cm. Pin-hole sizes of 5, 13, 15, 25 and 50 μm were tested. For a 5 μm pin hole the diffraction pattern was too small to study and only the first few rings were visible, which were insufficient for validation of the code. As pin-hole size increased, more rings became visible. At 50 μm, corresponding to the experimental data of Schaub *et al* [20], the first four rings had high visibility and adequate SNRs. A point of interest is that, when an uncollimated beam was used, effects of defocus were more noticeable, qualitative differences being visible for movements of as little as 10 μm, whereas for a collimated beam qualitative changes were visible only for 20 μm movement. This is consistent with theoretical calculations and also with simplified calculations and experimental results dating back to 1970 using a simplified Fraunhofer treatment [36], showing that the plane wave sensitivity to defocus is less than that for spherical wavefronts, Gaussian wavefronts having a sensitivity in between those for these two cases.

The next step in the research was to devise a method by which to work with particles. The main problem to be solved is that of working with a single particle at a given time and at a fixed position in space, with a particle size measured with microscopic techniques. To derive three-dimensional information, data from the x–y position and the diffraction pattern are used to yield the out-of-plane component. For this, sphericity of the particles must be assumed, so seeding with pollen, which is not spherical, was not studied. To start with, spherical glass and polystyrene particles were used.

Several methods for isolating a single particle were tried. A layer of monodisperse polystyrene spheres was deposited onto a slide, with a range of sizes from 3 to 13 μm tested. However, some problems were encountered because the solvent in which the polystyrene spheres were held evaporated, leaving cloudy contours on the slide surface. This noise precluded an accurate measurement of diffraction rings. Some were isolated and could be investigated but, when the defocus was increased, nearby particles caused problems. This approach was abandoned.

Glass particles not suspended in a solvent were used in sizes from 4 to 150 μm. Particles small enough to be of interest and large enough to be easy to handle, in the range 10–30 μm, were selected from this distribution. These particles were deposited onto a slide and stuck to

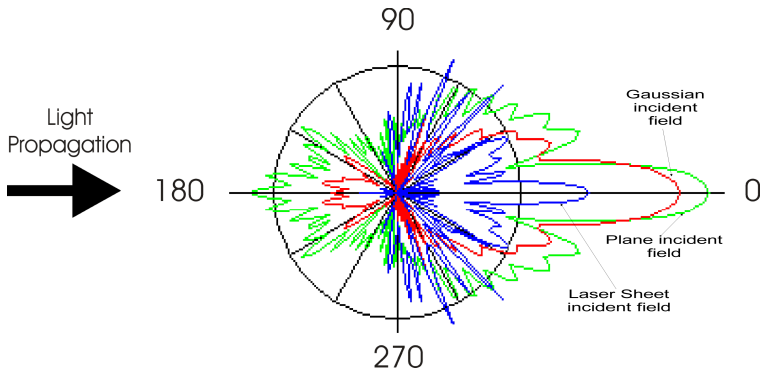

Figure 3. The normalized scattering pattern for a water particle 5 μm in diameter suspended in air, obtained using various incident wavefields ($\lambda = 532$ nm, complex index of refraction $n = 1.3372 + 1.4991 \times 10^{-9}$i).

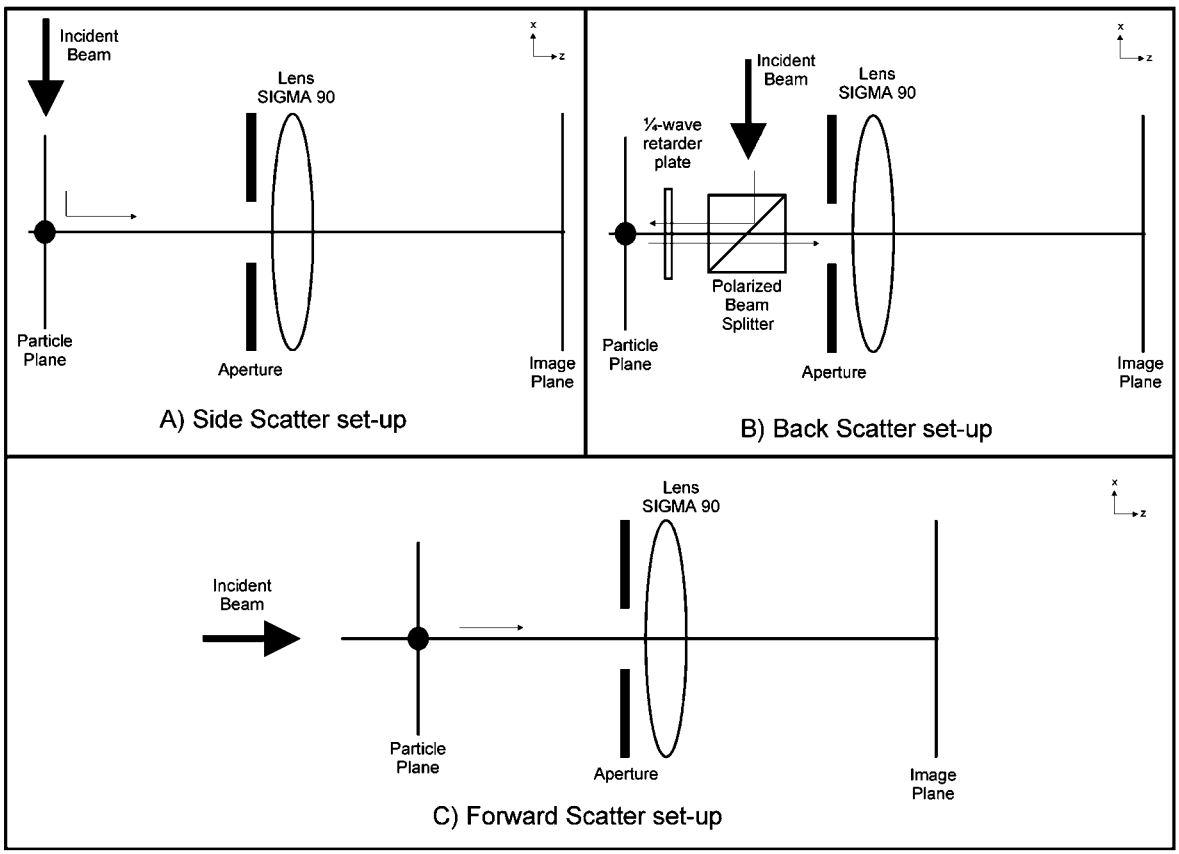

Figure 4. The experimental set-up. The object plane is at 102 mm and the image plane is at 801 mm from the lens. In back scattering configuration, one must add 19 mm to the object plane distance in order to compensate for the prism optical path difference.

the glass surface by leaving some residual humidity on the slide. This arrangement worked well for forward scattering and for large particle sizes. For smaller sizes, the system did not yield adequate ring definition due to noise. So, initially the larger 18 μm particles were selected. Tests were carried out for three scattering configurations (back, forward and side scattering), each employing three illumination wavefronts (plane, Gaussian and a sheet of light). For the three configurations, the distance between particle image rings appeared unaltered, qualitatively, on using different wavefronts for particle illumination, because they were all at the same out-of-focus distance. However, an overall difference in intensity was recorded when using the three illumination wavefronts. This intensity variation is given by illumination wavefronts, not by the incident beam intensity, according to our numerical model.

In forward scattering, the noise was less than expected, whereas both the diffracted light from the particle and the undiffracted background light intensity had to be adjusted to match them to the CCD camera gain in order to avoid saturation. In back scattering, the noise increased primarily due to the fact that the scattering field goes through more optical elements. Qualitatively, the images were similar to those for forward scattering.

The interesting point to note for the side scattering case was that the number of rings did vary significantly

compared with those in back and forward scattering. This effect is due to the asymmetry of the particle field in side scattering, needing a full aperture calculation rather than a simplified radial calculation. Moreover, these scattering characteristics vary over a very narrow angular movement such that the particle image varies with even a small angular displacement, making the matching of side scattering velocimetry images with theoretical predictions with sufficient accuracy almost impossible, given the uncertainties in experimental parameters.

In order to compare the results obtained here with those obtained by other workers, particle images for forward scattering were selected for comparison with theoretical calculations using GLMT, other experimental data and image predictions using other codes such as that of the University of Nebraska as well as existing classical Lorenz–Mie code.

With the expected CCD camera noise and experimental variations, the results presented here are encouraging in that they were very close to those obtained by Schaub *et al* [20], both in terms of the experimental images and in terms of numerical calculations for a comparable image size. Note, however, that the results reported in this paper are the first for which a quantitative comparison of numerical predictions and experimental images has been given. Figures 5(*a*)–(*c*) show enhanced experimental particle images for three viewing configurations (forward, side and back scattering). The particle size is 18 μm and the particle is located 2.0 mm out of focus relative to the lens. Figures 5(*d*)–(*f*) show enhanced experimental particle images in side-scatter viewing for a Gaussian beam, a light sheet and a plane wavefront respectively. In this case the particle is located 1.5 mm out of focus. As previously stated, these images are similar but of varying intensity.

An important aspect of the research was a preliminary study of the most significant sources of error, both with a view to minimizing them and to estimate the likely sensitivity and accuracy of the method. There are five main types of error involved in this experiment.

(i) Mathematical modelling of a physical problem: because of the complexity of the physical problem, various simplifying assumptions which have an impact on the ultimate accuracy of the technique are made. These involve assumptions about particle characteristics such as homogeneity and non-magnetic, symmetry assumptions, the thin-lens approximation, Seidel aberrations and that the collision between the wavefront and the particle is elastic. A great deal of effort has been made in order to create a model of the scattering process so that these simplifications are not significant.

(ii) Blunders: as computer programs become complex and lengthy, the existence of a small error in a program may be hard to detect and correct. There are basically two methods for dealing with errors of this kind, verification against a known answer and the breaking down of the program into modules and the testing of these separately. The GLMT toolbox was tested by testing each of its modules separately against established algorithms and other authors' calculated results and their software, when this was available. Moreover, the whole software was also validated against experimental results and predicted results produced by other authors.

(iii) Uncertainty in physical data: this is a major source of error since many physical constants of interest are not known with sufficient accuracy, such as the complex index of refraction, beam parameters, camera CCD pixel size, object and image distances and particle size. Here, we include camera noise since it results in an uncertainty in the measured intensity field.

(iv) Machine errors: these are errors inherent in using the floating point representation of numbers. Here we include also the imaging rounding error produced by CCD cameras as they record an image with a finite spatial and intensity scale. This imaging error is several orders of magnitude larger than the machine rounding error. For these tests, CCIR CCD cameras were used, having an eight-bit intensity range and a pixel size of approximately 10 μm with a total of 768×576 pixels. This factor contributed significantly to the measurement error.

(v) Mathematical truncation error: numerically solving a mathematical problem results in this kind of error, when an infinite process is approximated by a finite one. In this instance, the use of series expansions and numerical integration contributed significantly to this type of error.

Two further sources of error were identified but not accounted for in these first results: camera calibration involving bespoke tuning, noise calibration and correction for pixel sensitivity and the inclusion of the system modulation transfer function (MTF) in producing the calculated particle image. This is a complex problem, which is not well understood, that shall be treated in detail in a further publication.

A rough study of the above-mentioned factors was carried out, involving direct measurement when possible, numerical simulations to establish variances and numerical partial derivatives, analytical treatment and the use of published data. The results were combined to yield an estimate of the expected RMS error between the predicted and experimental images. The error was estimated to be at least six grey levels RMS.

Figures 6(*a*) and (*c*) shows experimental, not digitally processed, glass particle images (magnification 7.5 in a 101×101 pixels eight-bit TIFF image) of a 18 μm particle 1.5 mm out of focus and 1.5 mm into focus, respectively, for forward scattering, illuminated by a 1.5 mm, $\lambda = 0.6328$ μm Gaussian beam. They may be compared with the numerical predictions shown in figures 6(*b*) and (*d*) obtained using the GLMT. Figure 7 shows a radial intensity comparison between the experimental and the numerical prediction images given in figures 6(*a*) and (*b*). The quantitative RMS variation between them was measured to be 9.9 grey levels, compared with an expected minimum of six grey levels. It is believed that the camera calibration and MTF correction will yield a further 2–3 grey levels. The pixel sensitivity was not calibrated and camera noise can be considered to be approximately 1.0 grey levels RMS. For positional purposes, it is the relative position of diffraction rings which predominantly determines the accuracy. Germane to this technique is primarily determining

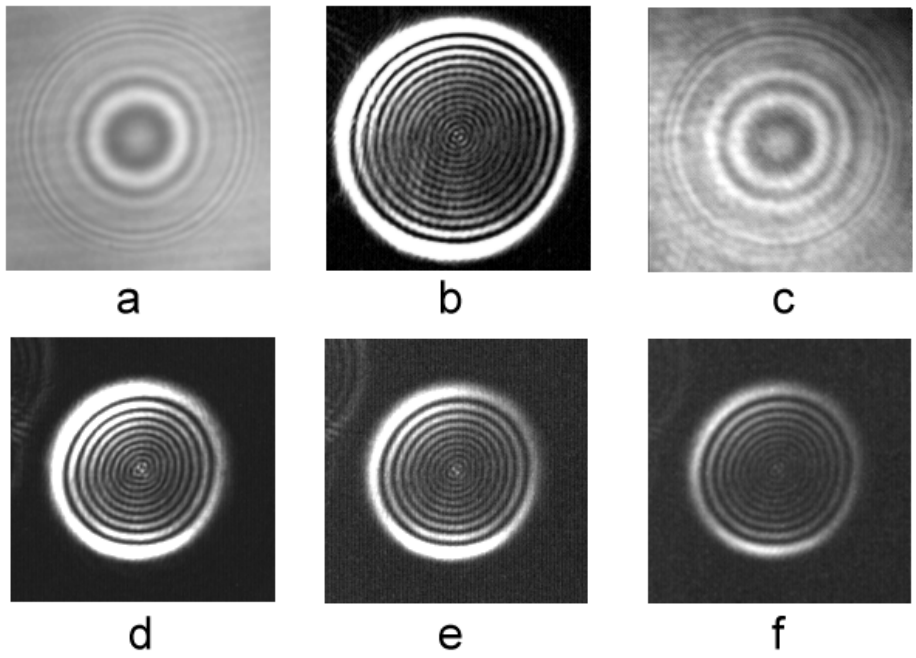

Figure 5. Experimental images for three viewing set-ups, according to figure 4 ((*a*) forward, (*b*) side and (*c*) back scattering) and three types of illumination for viewing side scattering ((*d*) a Gaussian beam, (*e*) a light sheet and (*f*) a plane wave).

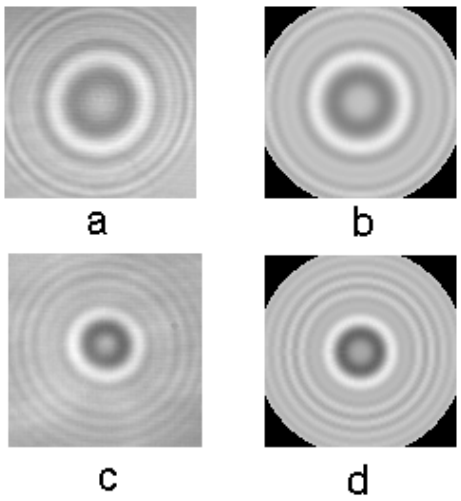

Figure 6. Comparisons of experimental and theoretical particle images of an 18 μm diameter glass bead in forward scattering: (*a*) the experimental particle image 1.5 mm after the focal plane, (*b*) the numerical prediction obtained using GLMT for the previous image, (*c*) the experimental particle image 1.5 mm before the focal plane and (*d*) the numerical prediction using GLMT for the previous image.

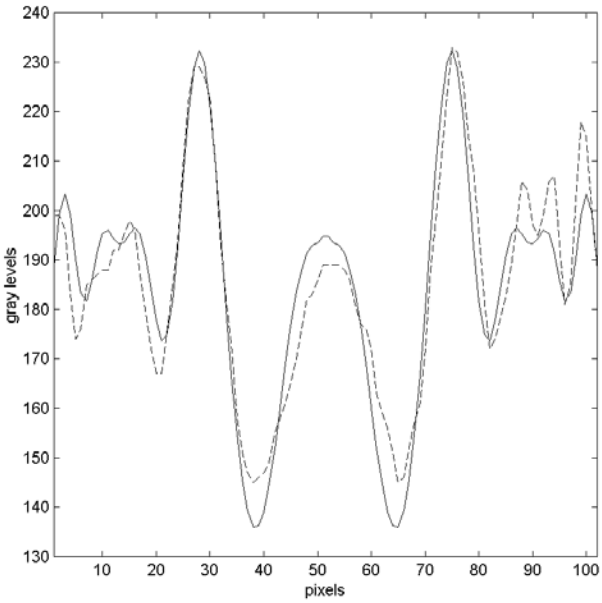

Figure 7. A radial intensity comparison of experimental (broken line) and numerical (full line) predictions for a 18 μm diameter glass particle image 1.5 mm after the focal plane.

the accuracy of out-of-plane position estimation, for the image above was estimated to be 5 μm out of plane. This accuracy can be increased at the cost of having a diminished region of interest [23]. For many velocimetry applications, for which the magnification is of the order of 1–3, the potential accuracy of this method is estimated to be 20–30 μm, using an approach of comparing predicted and experimental images and a Nelder–Mead optimization, though this may be increased with more sophisticated approaches to optimization.

6. Conclusions

The importance of considering the wavefront shape for each application has been illustrated. The need to include in the calculation provision for lens aberrations and the aperture shape is also a contribution which workers wishing to produce particle scattering codes need to consider.

Much work remains to be done on refining the code, speeding it up and extending it so that all forms of aberrations may be considered. However, having a quantitatively

accurate particle image model is a step forwards, particularly in velocimetry applications. This step forwards opens the way for routine accurate three-dimensional velocity estimation, by three-dimensional particle positioning from two-dimensional camera images.

The image data set for glass particles of 18 μm diameter obtained for the three illumination schemes and the three viewing positions mentioned and for the images calculated using GLMT is available from the corresponding author in raw format together with experimental parameters. This data set can be used to validate other scattering calculations for applications such as phase-Doppler techniques, particle sizing and velocimetry.

Acknowledgments

We would like to thank Professor Dennis R Alexander of the University of Nebraska for his help and advice on the computational techniques used in this paper. J A Guerrero and D Moreno gratefully acknowledge the scholarships granted by the CONACYT (Mexico). M Funes-Gallanzi wishes to thank the Royal Society of London for supporting the initial phase of this project, which we later completed with the kind support of Photon Imaging (USA) and ASCI SA de CV (Mexico).

References

[1] Gauthier V and Riethmuller M L 1988 Application of PIDV to complex flows: measurements of third component *Von Karman Institute Lecture Series* vol 6 (Rhode Saint Genese, Belgium: Von Karman Institute)

[2] Westerweel J and Nieuwstadt F T M 1991 Performance tests on 3-dimensional velocity measurements with a two-camera digital particle image velocimeter *ASME Laser Anemometry* **1** 349–55

[3] Gray C, Greated C A, McCluskey D R and Easson W J 1991 An analysis of the scanning beam PIV illumination system *Meas. Sci. Technol.* **2** 717–24

[4] Meng H and Hussain F 1991 Holographic particle velocimetry. A 3D measurement technique for vortex interactions, coherent structures and turbulence *Fluid Dynamics Res.* **8** 33–52

[5] Brüker Ch and Althaus W 1992 Study of vortex breakdown by particle tracking velocimetry (PTV). Part 1: bubble-type vortex breakdown *Exp. Fluids* **13** 339–49

[6] Bryanston-Cross P J, Funes-Gallanzi M, Quan T R and Judge T R 1992 Holographic particle image velocimetry (HPIV) *Opt. Laser Technol.* **24** 251–6

[7] Dinkelaker F, Schaffer M, Ketterle W and Wolfrum J 1992 Determination of the third velocity component with PTA using an intensity graded light sheet *Exp. Fluids* **13** 357–9

[8] Willert C E and Gharib M 1992 Three-dimensional particle imaging with a single camera *Exp. Fluids* **12** 353–8

[9] Ovryn B and Hovenac E A 1993 Coherent forward scattering particle image velocimetry: application of Poisson's spot for velocity measurements in fluids *Proc. SPIE* **2005** 338–48

[10] Prasad A K and Adrian R J 1993 Stereoscopic particle image velocimetry applied to liquid flows *Exp. Fluids* **15** 49–60

[11] Adrian R J, Meinhart C D, Barnhart D H and Papen G C 1993 An HPIV system for turbulence research *Proc. ASME* **148** 17–21

[12] Guezennec Y G, Zhao Y and Gieseke T J 1994 High-speed 3D scanning particle image velocimetry (3-D PIV) technique *Proc. 7th Int. Symp. on Applications of Laser Techniques to Fluid Mechanics, Lisbon* pp 26.2.1–10

[13] Prasad A K and Jensen K 1995 Schiempflug stereocamera for particle image velocimetry in liquid flows *Appl. Opt.* **34** 7092–9

[14] Hinsch K D 1995 Three-dimensional particle velocimetry *Meas. Sci. Technol.* **6** 742–53

[15] Allano D, Lecerf A and Trinite M 1998 High resolution PIV applied to 3D component velocity measurements *Report 06PT18* Contract BriteEuram BR.PR-CT95-0118

[16] Raffel M, Westerweel J, Willert C, Gharib M and Kompenhans J 1996 Analytical and experimental investigations of dual-plane particle image velocimetry *Opt. Engng* **35** 2067–74

[17] Funes-Gallanzi M 1998 High accuracy measurement of unsteady flows using digital PIV *Laser Opt. Technol.* **30** 349–59

[18] Padilla Sosa P and Funes-Gallanzi M 1999 High accuracy at low magnification 3D PIV measurement using the concept of locales *Laser Opt. Technol.* submitted

[19] Wiles K J 1985 Development of a system for secondary liquid injection into a Mach 2 supersonic flow to study drop size and distribution by video imaging techniques *Master's Thesis* University of Nebraska, Lincoln

[20] Schaub S A, Alexander D R and Barton J P 1989 Theoretical model for the image formed by a spherical particle in coherent imaging system, comparison to experiment *Opt. Engng* **23** 565–71

[21] Seeman M P 1987 Aerosol characterization using a PDPA and laser imaging/video processing system *Master's Thesis* University of Nebraska, Lincoln

[22] Schaub S A, Alexander D R and Barton J P 1991 Theoretical model of the laser imaging of small aerosols: applications to aerosol sizing *Appl. Opt.* **30** 4777–84

[23] Ovryn B, Wright T and Khaydarov J D 1995 Measurement of three-dimensional velocity profiles using forward scattering particle image velocimetry (FSPIV) and neural net pattern recognition *Proc. SPIE* **2546** 112–23

[24] Adrian R J and Yao C S 1983 Development of pulsed laser velocimetry for measurement of fluid flow *Proc. 8th Biennial Symp. of Turbulence* ed G Patterson and J L Zakin (Rolla: University of Missouri)

[25] Gouesbet G and Gréhan G 1982 Sur la généralisation de la théorie de Lorenz–Mie *J. Optique* **13** 97–103

[26] Gouesbet G, Maheu B and Gréhan G 1998 Light scattering from a sphere arbitrarily located in a Gaussian beam, using a Bromwich formulation *J. Opt. Soc. Am.* A **5** 1427–43

[27] Moreno D, Mendoza Santoyo F, Funes-Gallanzi M and Guerrero J A 1999 Particle positioning from a single CCD image for application to velocimetry: theory and comparison to experiment *Appl. Opt.* submitted

[28] Debye P 1909 Der Lichtdruck auf Kugeln von beliebigem Material *Ann. Phys., Lpz.* **30** 57–136

[29] Mie G 1908 Beiträge zur Optik trüber Medien, speziell kolloidaler Metallösungen *Ann. Phys., Lpz.* **25** 377–445

[30] Goodman J W 1968 *Introduction to Fourier Optics* (New York: McGraw-Hill)

[31] Ren K F, Gréhan G and Gouesbet G 1994 Electromagnetic field expression of a laser sheet and the order of approximation *J. Optique* **25** 165–76

[32] Abramowitz M and Stegun I A (eds) 1972 *Handbook of Mathematical Functions* (New York: Dover) pp 332–4

[33] Dave J V 1969 Scattering of the electromagnetic radiation by large absorbing sphere *IBM J. Res. Dev.* **13** 302–13

[34] Gréhan G, Gouesbet G, Guilloteau F and Chevaillier J P 1992 Comparison of the diffraction theory and the generalised Lorentz–Mie theory for sphere arbitrarily located into a laser beam *Opt. Commun.* **90** 1–6

[35] Hale G M and Querry M R 1973 Optical constants of water in the 200 nm to 200 microns wavelength region *Appl. Opt.* **12** 555–63

[36] Menzel R and Shofner F M 1970 An investigation of Fraunhofer holography for velocimetry applications *Appl. Opt.* **9** 2073–9